University of Texas at El Paso
ScholarWorks@UTEP

Open Access Theses & Dissertations

2022-12-01

Direct Ink Write And Thermomechanical Characterization Of Thermoset Composites

Sergio Dante Favela
University of Texas at El Paso

Follow this and additional works at: https://scholarworks.utep.edu/open_etd

Part of the Mechanical Engineering Commons, and the Polymer Chemistry Commons

Recommended Citation

Favela, Sergio Dante, "Direct Ink Write And Thermomechanical Characterization Of Thermoset Composites" (2022). *Open Access Theses & Dissertations*. 3670.
https://scholarworks.utep.edu/open_etd/3670

This is brought to you for free and open access by ScholarWorks@UTEP. It has been accepted for inclusion in Open Access Theses & Dissertations by an authorized administrator of ScholarWorks@UTEP. For more information, please contact lweber@utep.edu.

DIRECT INK WRITE AND THERMOMECHANICAL CHARACTERIZATION OF HIGH-PERFORMANCE THERMOSETS

SERGIO DANTE FAVELA

Master's Program in Mechanical Engineering

APPROVED:

Yirong Lin, Ph.D., Chair

Tzu-Liang Tseng, Ph.D., Co-Chair

Jaime Regis, Ph.D.

Stephen L. Crites, Jr., Ph.D.
Dean of the Graduate School

Copyright ©

by

Sergio Dante Favela

2022

Dedication

To my mother Marcela, the woman who has supported me through my whole journey ever since taking my first baby steps. Thank you, mom, for all your sacrifices and love you've given me all these years. To my aunt Gabriela and grandmother Beva, who raised and cared for me alongside my mother throughout my whole life. To my extended family Hugo, Hugo Jr., and Cecily, for their support and friendship for so many years. To my friends Saul, Alan, Jezel, Dalia, Marco, Daneli, Cesar, Abril, Irvin, Naomi Alexis, Aaron, and Sofia, for all the unforgettable adventures and experiences that we shared during college. And to all the people who've, through their continuous support, allowed me to become who I am and complete this academic milestone.

DIRECT INK WRITE AND THERMOMECHANICAL CHARACTERIZATION OF THERMOSET COMPOSITES

by

SERGIO DANTE FAVELA, B.S.

THESIS

Presented to the Faculty of the Graduate School of

The University of Texas at El Paso

in Partial Fulfillment

of the Requirements

for the Degree of

MASTER OF SCIENCE

Department of Aerospace and Mechanical Engineering

THE UNIVERSITY OF TEXAS AT EL PASO

December 2022

Acknowledgements

I'd like to start by thanking my mentor Dr. Lin, who allowed me to join his research group back in 2020. Under his research team and leadership, I was able to learn far beyond what I was expecting when I initially joined the research team. All these experiences have allowed for me to become a more well-rounded engineer. Not limited to technical knowledge, I was able to develop my communication skills, presentation skills, and teamwork abilities. I am forever grateful for all the opportunities which I've been able to obtain thanks to the experience gained during being a participant of his research group.

I'd like to thank Dr. Tseng for allowing me to expand my knowledge in the field of non-destructive evaluation by appointing me as the lead member for composite inspection and manufacturing. The challenges during the project have allowed me to develop new solutions and truly allowed me to implement solutions to real world problems.

I'd like to thank Dr. Regis for being a member of my committee, a friend, and a mentor during previous research project while working with the smart materials processing research group.

I'd like to thank my lab mates Alexis, Sofia, Aaron for all their continuous support during research projects and for being incredible friends outside the working environment. Thanks for making research even more fun than it already is.

Lastly, I'd like to thank the aerospace center, the department of mechanical engineering, the department of industrial manufacturing and systems engineering, Lockheed Martin aeronautics, and Kansas City National Security Campus, for allowing me to participate in research projects that have made me grow both professionally and personally.

Abstract

This research will be divided into two sections. The first section discusses direct ink writing and thermomechanical characterization for thermoset composites. The thermoset ink is prepared with fillers aiding the printing process by modifying the rheology of the ink and geometry retention by allowing for the part to have an initial UV cure step. Three specimen formulations with different weight percentages were printed by material extrusion in the shape of tensile specimens following ASTM standard D638 to characterize the mechanical properties at room temperature, 100°C and 200°C. Furthermore, the ink resin was characterized through DSC, TGA, and rheology testing. The second section will discuss the detection of intentional defects on both curved and planar carbon fiber composites through non-destructive evaluation (NDE) methods. The main NDE technique used is ultrasonic testing (UT) by using a phased array probe. Different planar and curved composites were produced by compression pressing and molded vacuum bagging. UT was used to detect defects such as delaminations and inclusions at different layers, locations, and sizes. The data acquired from the composite panels was utilized to train an AI model to detect the category of defects, location, and depth.

Table of Contents

Dedication iii

Acknowledgements v

Abstract vi

Table of Contents vii

List of Figures x

Chapter 1: Direct Ink Write of UV Curable Thermoset Resins 1

- Introduction 1
- Experimental Methods 5
  - DIW Ink Preparation 5
  - Curing Schedule 6
  - Rheology Testing 6
  - Oscillation Characterization 7
  - Thermogravimetric Analysis (TGA) 8
  - Dynamic Mechanical Analysis (DMA) 10
  - Interpenetrating Polymer Networks (IPN) 13
  - DIW printing of PT-30/Acrylate Samples 14
  - Tensile Testing at Elevated Temperatures 17
- Results 19
  - Testing at Room Temperature 19
  - Testing at 100°C 20
  - Testing at 200°C 20
- Conclusion 21
- Future Work 21

Chapter 2: Non-Destructive Evaluation and Testing of Carbon Fiber Curved Composites 23

- Introduction 23
- Experimental Methods 24
  - Composites Manufacturing 24
  - Ultrasonic Testing Equipment 27
- Results 28

Conclusion 30
Future Work 31
References 32
Vita 35

List of Tables

Table 1.1: Room Temperature Testing Results 19

Table 1.2: 100°C Testing Results 20

Table 1.3: 200°C Testing Results 21

List of Figures

Figure 1.1: Schematic of an FDM 3D Printer 2

Figure 1.2: Schematic of an DIW 3D Printer 2

Figure 1.3: Molecular Structure of Polymers 3

Figure 1.4: Thermoplastics and Thermosets Comparison 3

Figure 1.5: Crystalline and Amorphous Polymers Volume v Temperature Graph 4

Figure 1.6: Cyanate Ester Structures 5

Figure 1.7: Flow Curves for PT-30/Acrylate Inks with Different Garamite Percentages 7

Figure 1.8: Complex Shear Modulus Curves of PT30 Inks with 4% Garamite 8

Figure 1.9: TGA of PT-30 at Different Cure Stages 9

Figure 1.10: TGA of PT-30/Acrylate Inks at different cure stages 10

Figure 1.11: DMA of Fully Cured PT-30 samples 11

Figure 1.12: DMA of UV Cured PT-30/Acrylate Samples 12

Figure 1.13: DMA of Thermally Cured PT-30/Acrylate Samples 13

Figure 1.14: Two-step curing process for PT-30/Acrylate 13

Figure 1.15: a) KR2-15 Printhead b) Hyrel System 30M Printer 14

Figure 1.16: Tensile Testing Specimens for ASTM D638 15

Figure 1.17: a) Printing Pattern b) Finalized Green Part Prints 16

Figure 1.18: Print Head UV Array 16

Figure 1.20: Successfully Printed Specimens 17

Figure 1.21: Instron Load Cell and Enviromental Chamber 18

Figure 1.22: Tensile Specimen with Valid Tensile Failure 19

Figure 1.23: DIW Specimens with Added Milled Carbon Fiber 22

Figure 2.1: NDT Schematic 24

Figure 2.2 Composite Mold CAD Models..... 25

Figure 2.3 Composite Layup with Vacuum Applied..... 26

Figure 2.4: Carbon Fiber Composite Embedded Defects 26

Figure 2.5: Manufactured Carbon Fiber Composites 27

Figure 2.6: NW-1 Probe and its Components..... 27

Figure 2.7: Omniscan Scan Readings 28

Figure 2.8: a) B-Scan Displaying Walls b) B-Scan Displaying Defects 29

Figure 2.9: Image Labeling Process..... 30

Figure 2.10: a) Defect detection in the C-Scan b) Defect and Wall detection in the B-Scan..... 30

Chapter 1: Direct Ink Write of UV Curable Thermoset Resins

INTRODUCTION

There has been an increased interest in additive manufacturing (AM) technologies, also known as 3D printing, due to their ability to create complex designs not commonly accessible to traditional manufacturing methods. This paper focuses on the AM process category of material extrusion (MEX) specifically on the technology of Direct-Ink-Writing (DIW). DIW is an extrusion-based additive manufacturing method which focuses on the printing of materials known as "inks", these materials are typically in a liquid state and can be printed at room temperature by being deposited along a substrate following the paths defined from a 3D structure. [1] Some of the main differences for DIW when compared to fused deposition modeling (FDM) is its ability to deposit material in room-temperature environments in the form of an ink, to build complex structures. [2] The technologies of DIW and FDM are used to print synthetic polymers. However, the FDM technology focuses on printing on thermoplastic polymers; in contrast, the DIW technology focuses on printing thermosets, ceramic slurries, and practically any material that can be engineered to demonstrate the appropriate rheological behavior.[3] Furthermore, DIW technologies typically use a pneumatic control system to extrude materials from a reservoir. FDM systems use feeding gears to grip and pass the filament through a heater block which melts the thermoplastic material. The figure below represents and contrast the schematics for FDM and DIW.

1
2
3

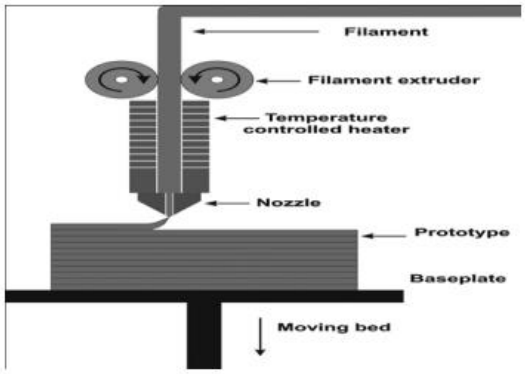

Figure 1.1: Schematic of an FDM 3D Printer[4]

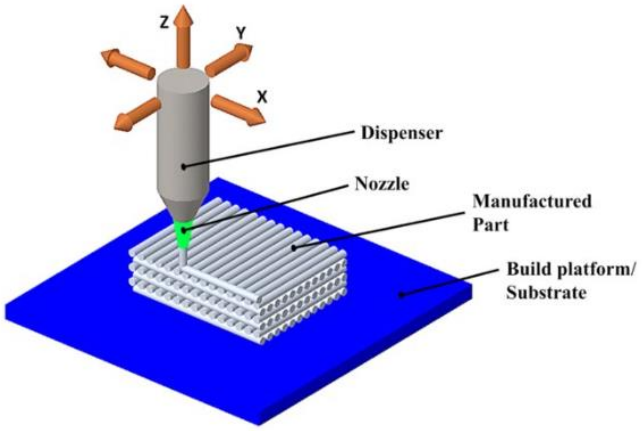

Figure 1.2: Schematic of an DIW 3D Printer[5]

Contrasting the extrudable polymers used for both material extrusion systems, the thermoplastics solidify as they cool down after being melted and selectively deposited. These thermoplastics can be melted and re-shaped as many times as desired. However, the thermosets experience a process known as crosslinking during the curing process, which is an irreversible process allowing for the molecules to chemically bond. The thermoset materials are made up of monomers and pre polymers which bond allowing for the networks to polymerize, creating the crosslinked networks. The crosslinks formed during curing are not present in thermoplastics. Figure 1.3 demonstrates an illustration comparing the molecular structures for thermoplastics and thermoset polymers.

4

5

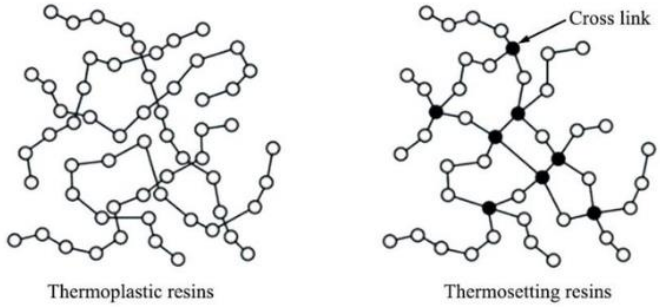

Figure 1.3: Molecular Structure of Polymers[6]

The curing process for the thermoplastic materials is completely reversible and no chemical bond occurs. These crosslinks allow for the thermosets to achieve incredible strengths and environmental resistance, being far superior at high temperature applications as opposed to thermoplastic materials. Furthermore, these crosslinks allow for thermosets to obtain high levels of resilience, chemical resistance, typically suited for aerospace applications. Although, the thermoplastic materials still exhibit superiority in its recyclability and reshaping factor.

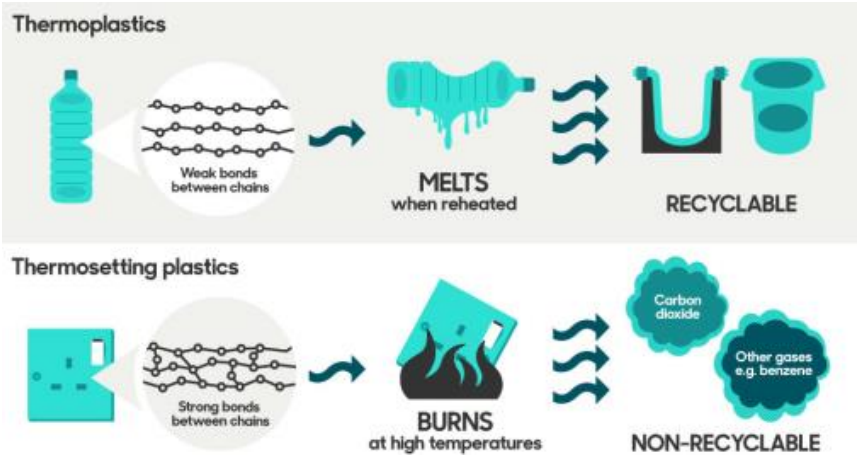

Figure 1.4: Thermoplastics and Thermosets Comparison[7]

6
7

Cyanate esters are a group of thermosetting resins exhibiting a high glass transition temperature. The cyanate ester materials have been a focus in research due to their processability as compared to thermoset epoxies and their high thermal stability. The glass transition temperature is the mid-point at which the amorphous polymer, in this case the thermoset, will shift from a glassy state into a rubbery state. During this rubbery state the material is softened although it does not experience melting.

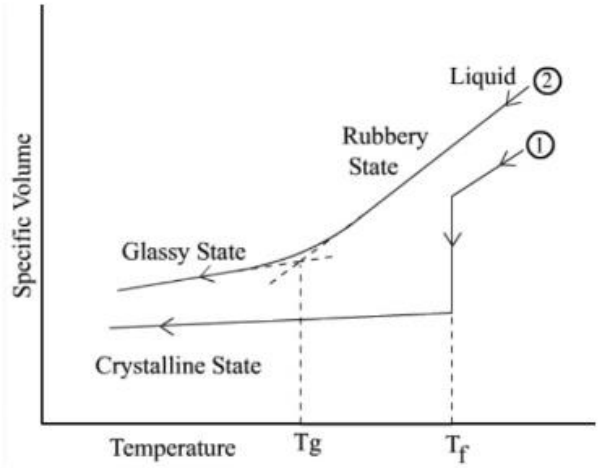

Figure 1.5: Crystalline and Amorphous Polymers Volume v Temperature Graph[8]

Cyanate esters typically form through the curing of two functional cyanate end groups through a process known as cyclotrimerization. The cyclotrimerization occurs with the addition of a metal catalyst or by the addition of temperature. This process allows for the creation of aromatic rings, giving the polymers its high strength and temperature resistance. For cyanate triazine structures, which are highly temperature resistant, are formed by cyanate end groups linking through oxygen bonds during the curing process. This characteristic enables these resin systems to achieve a thermal degradation temperature occurring at around 450°C.[9]

8
9

Figure 1.6: Cyanate Ester Structures[10]

Due to the before-mentioned high thermally properties, high glass transition temperature, high strength, chemical resistance, and excellent dielectric properties. These cyanate ester polymers are typically used in a variety of applications and industries, including microelectronics, aircraft, aerospace, automotive, missiles, and antennae.

This research will explore the ability to include fillers aiding in the printability and processability of high thermal performance polymers such as cyanate esters for direct ink write technologies. Furthermore, the prepared inks will be characterized thermo-mechanically to analyze their behavior as temperature is increased. This works aims to provide a comprehensive understanding of the performance of high temperature performance thermosets and their application in advanced industries.

EXPERIMENTAL METHODS

DIW Ink Preparation

The manufacturing of printable ink resins includes 4 components. The major components included a cyanate ester resin commercially known as Primaset PT-30 (Arxada, Switzerland). A homopolymer known as Tri (2-hydroxyethyl) isocyanurate triacrylate (Sigma-Aldrich, USA, St. Louis, MO) which outclasses the glass transition temperature of other acrylate polymers. A chemical known as Garamite serving as a rheology modifier and providing structural support to

10

the printed objects. The last component was a photo-initiator which created crosslinks with the acrylate as the ink was exposed to UV light. Different formulations were produced to analyze the weight percentage effect on the mechanical properties of the printed specimens. Ratios of 50/50, 70/30, and 85/15 with increasing PT-30 content, were created.

Curing Schedule

PT-30 alone and inks prepared with different weight percentages followed the same thermal curing schedule as further described in this paragraph. Samples were thermally cured following a curing schedule of keeping the samples at 150°C for 1 hour, followed by applying 200°C for 3 hours. At this point the samples have completely solidified, obtaining a brownish orange color. After the cure, a post-cure step is applied to fully obtain the desired thermal properties by keeping the samples at 260°C for 1 hour. Inks prepared with acrylate and other fillers follow the same curing schedule being preceded by a UV curing step applying the UV wavelength of 365nm for 10 minutes after the samples have been printed.

Rheology Testing

Inks without the Garamite modifier exhibit a Newtonian flow behavior. Garamite was added to induce a thixotropic effect allowing for the fluid to become fluid as a shear load is applied. This phenomenon is otherwise described as shear-thinning, which is desired for DIW. Figure 1.7 better demonstrate the behavior of inks as increased percentages of Garamite are added.

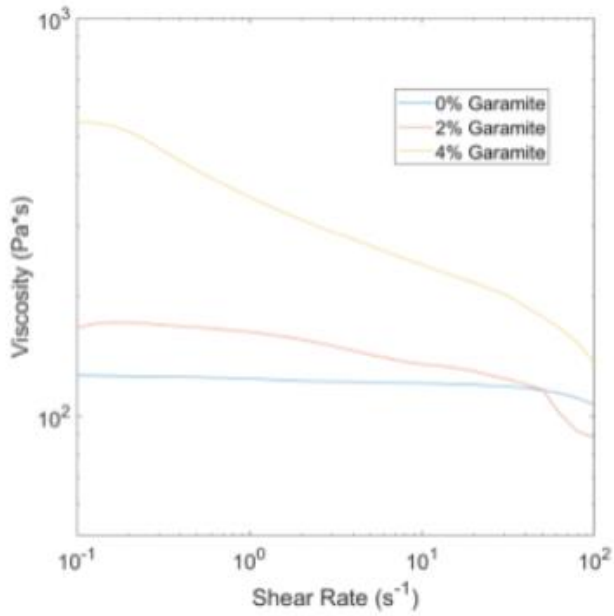

Figure 1.7: Flow Curves for PT-30/Acrylate Inks with Different Garamite Percentages

As observed from the flow curves, there is clear evidence that at increased Garamite percentages the shear-thinning effect is much more pronounced. However, inks with no Garamite content exhibit a low viscosity and Newtonian behavior. This would cause for the inks to flow out of the print nozzle, leading to no control over flowability of the material. Furthermore, no Garamite content led to spreading of the inks after being deposited and little self-support capabilities. Still with the Garamite being incorporated into the inks, the UV curing was still required as the structures were printed to prevent any spreading and collapsing of the structure.

Oscillation Characterization

Oscillation characterization for inks with 4% Garamite content was conducted to observe the behavior of the complex shear modulus. As observed in Figure 1.8, across all the oscillations ranges the storage modulus is greater than then loss modulus by nearly one order of magnitude. This indicates that the inks would flow freely even in the absence of applied shear stress.

Therefore, inks with increased Garamite content would be necessary to obtain self-supporting capabilities with minimal UV curing.

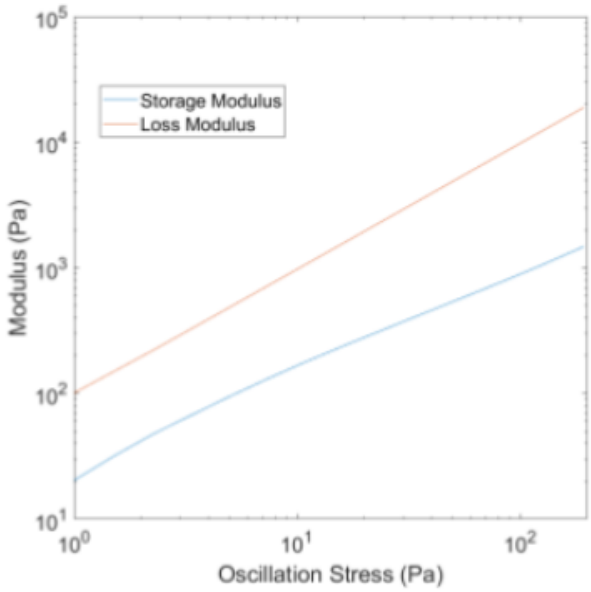

Figure 1.8: Complex Shear Modulus Curves of PT30 Inks with 4% Garamite

Thermogravimetric Analysis (TGA)

TGA was performed on both, inks at different cure stages and PT-30 resin under different curing environments to analyze the mass loss at elevated temperatures. Figure 1.9 shows the TGA graphs for PT-30 at different curing environments and stages. Uncured samples had a mass loss of around 27% at a temperature of around 150°C for tests done under oxygen and nitrogen environments. PT-30 that was cured until 200°C does not exhibit the same thermal resistance as post-cured samples and a mass loss of around 10% is observed at around 175°C. PT-30 cured to 260°C, following a curing schedule of 150°C for 1 hour, 200°C for 3 hours, and a post-cure at 260°C for 1 hour shows a better thermal resistance losing around 18% mass at 400°C. Still, there is an initial mass loss of 2% for samples post cured at 260°C due to some uncured cyanate groups degrading.

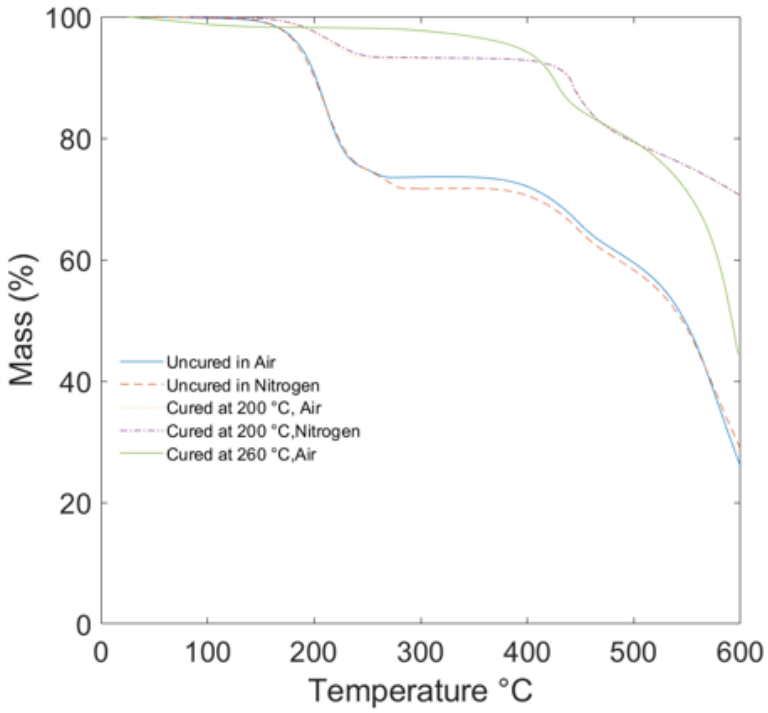

Figure 1.9: TGA of PT-30 at Different Cure Stages

TGA was performed for the inks at different cure stages as well. TGA was performed in an air environment for inks which were only UV cured, inks being cured at 200°C and inks post-cured at 260°C. Figure 1.10 shows the TGA curves of these three inks under curing conditions. For inks which were only UV cured, there is a mass loss of around 10% experienced at a temperature of 230°C. This mass loss can be attributed to cyanate end-groups degradation due to the thermal cure not being applied. The incorporation of acrylate resulted in a mass loss of 5% up until the temperature of around 380°C being a lower temperature than that at which Pt-30 alone starts degradation. Pt-30 by itself I still able to better retain its mass at higher temperatures, as seen from comparing both graphs at temperatures above 400°C. However, the degradation temperatures shown by TGA demonstrate the competitive thermal resistance that the prepared inks possessed while being applicable for additive manufacturing technologies. However, it's

important to consider that greater percentages of PT-30 will allow for the inks to retain more of their mass as temperature is increased.

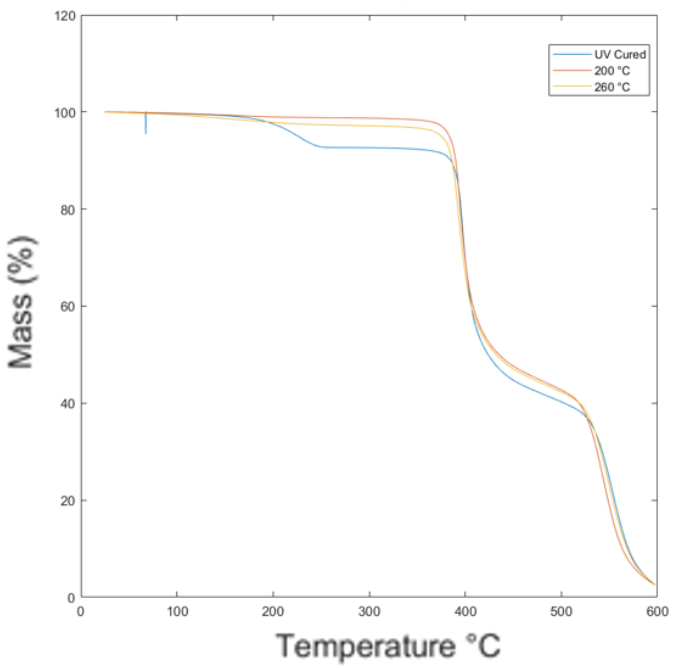

Figure 1.10: TGA of PT-30/Acrylate Inks at different cure stages

Dynamic Mechanical Analysis (DMA)

Similarly, to TGA, DMA sample were prepared by casting rectangular samples out of manufactured inks and pure PT-30. As seen in figure 1.11 DMA testing was performed on samples made of PT-30 only, which went through the entire curing process. The graphs represent an initial steady decrease in storage modulus changing from 2.90 GPa to 1.25 GPA. After reaching a temperature of 300°C, the storage modulus stabilizes until we see a decrease at the temperature of 380°C, which indicates that the glass transition temperature of the material is above 405°C. From the TGA results, testing was not done at higher temperatures than 405°C to avoid decomposition and possibly contaminating testing equipment. However, the results still demonstrate that the polymer can maintain its high mechanical properties at elevated

temperatures. Due to the limitations of the test, the peaks of the loss modulus and the tan delta were not reached.

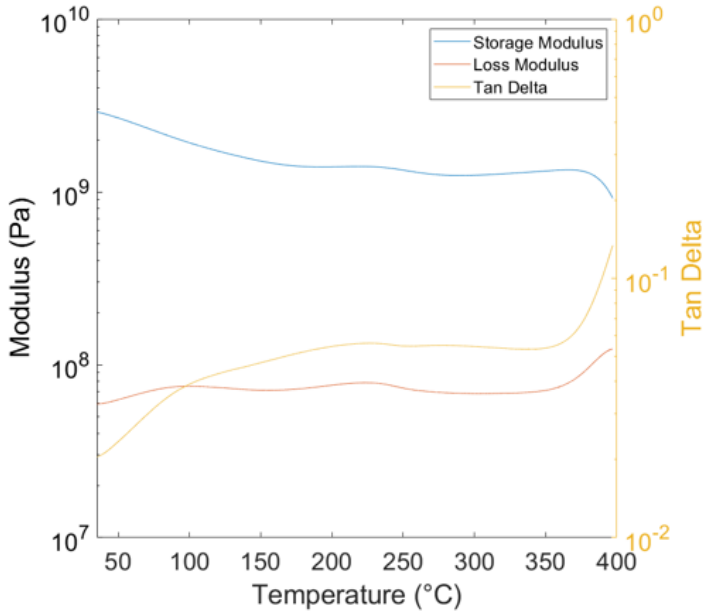

Figure 1.11: DMA of Fully Cured PT-30 samples

DMA done on inks consisted of testing done for samples which only went through UV curing and samples which completed the thermal curing along with the UV cure. Figure 1.12 shows the curve results for the specimens which exclusively went through the UV cure. From the DMA results, a fluctuation can be observed in the mechanical properties of the prepared ink materials. The UV-cured samples show two main peaks which correspond to the main polymer components. These peaks represent the glass transition temperatures for PT-30 and Acrylate. We initially see the first glass transition temperature for Acrylate occurring near the 200°C temperature and a second peak near the 300°C temperatures at which some mass loss was previously observed during TGA testing.

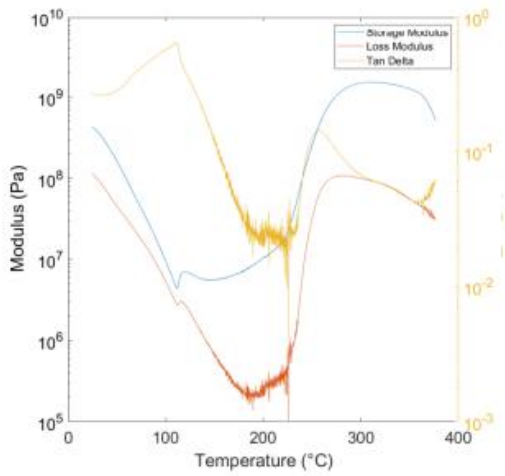

Figure 1.12: DMA of UV Cured PT-30/Acrylate Samples

Lastly, DMA testing was done on PT-30/Acrylate samples that had gone through a post-curing process. Figure 1.13 shows the complex modulus for the cured sample. A similar peak was observed at the temperature of 300°C, confirming the glass transition temperature for the tested DMA samples. A similar behavior is observed where the storage modulus decreases at the degradation temperature is approached while the tan delta increases, which indicates the glass transition temperature. Comparing these results to PT-30 alone, there is a clear decrease in the glass transition temperature of the material, although the material is still able to retain its properties at high temperatures with a similar thermal degradation to pure pt-30. By comparing these results to the previous DMA on samples which were not cured thermally, we can see that only one tan delta peak is shown indicating a single glass transition temperature even if both of the polymer components were not chemically bonded. This confirms the ability of these two polymer systems to form an interpenetrating polymer network (IPN). Furthermore, these results demonstrate the potential that these polymers have in forming an IPN network while maintaining properties similar to pure PT-30.

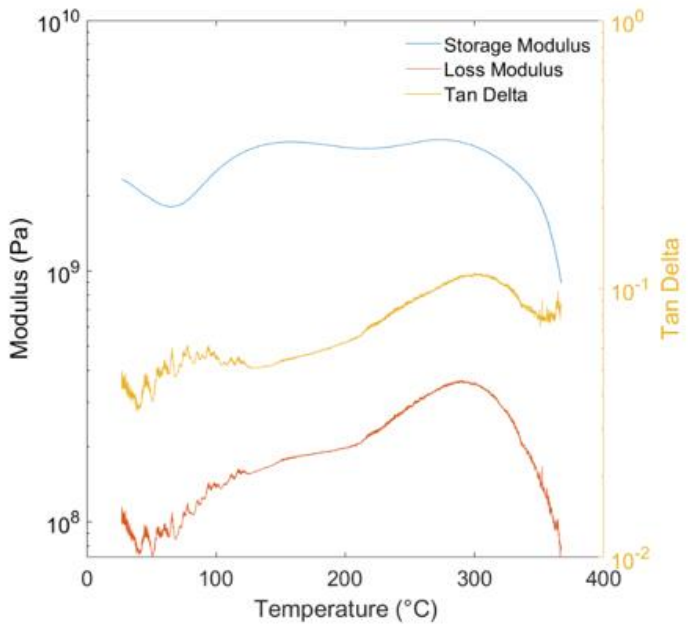

Figure 1.13: DMA of Thermally Cured PT-30/Acrylate Samples

Interpenetrating Polymer Networks (IPN)

In an interpenetrating polymer network polymers are combined without bonding together at the chemical level. This allows for both polymer systems to closely entangle together, becoming solid by forming two separate cross-linked networks while maintaining similar properties to their pure counterparts. This is one of the most popular methods for modifying cyanate ester resins and allowing for new functionalities to arise from introducing new cross-linked networks. The interpenetrating polymer networks allow for the 3D printing of high thermal performance thermosets by applying a two-step cure as depicted in Figure 1.14.

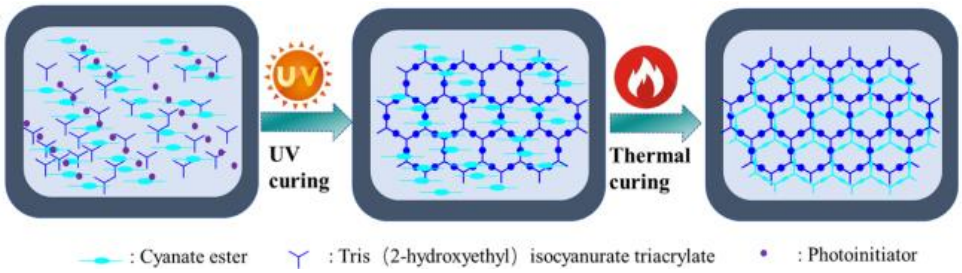

Figure 1.14: Two-step curing process for PT-30/Acrylate[11]

11

DIW printing of PT-30/Acrylate Samples

For the printing of all samples, a standard DIW printing system using the System 30 M printer along with a KR2-15 print head (Hyrel, USA, Norcross, GA). The KR2-15printhead is equipped with a software-controlled UV array system allowing for the duty control of the UV array from 0% to 100%. This facilitated the printing and consolidation of the print by commencing the crosslink process for the acrylate and the photo-initiator. The printer had the capability of using several print heads at once, allowing for multi-material printing. However, for this experiment a single print head was used. The printhead consisted of a stainless-steel reservoir, PCBs, which connected the print head to the printer, and a stepper motor which applied torque to push down on the reservoir and extrude material. The reservoir had a variety of tip attachments; for this experiment the tapered tip nozzles of 18 gauge were used to print specimens. Figure 1.15 shows illustrations for the printhead and printing system.

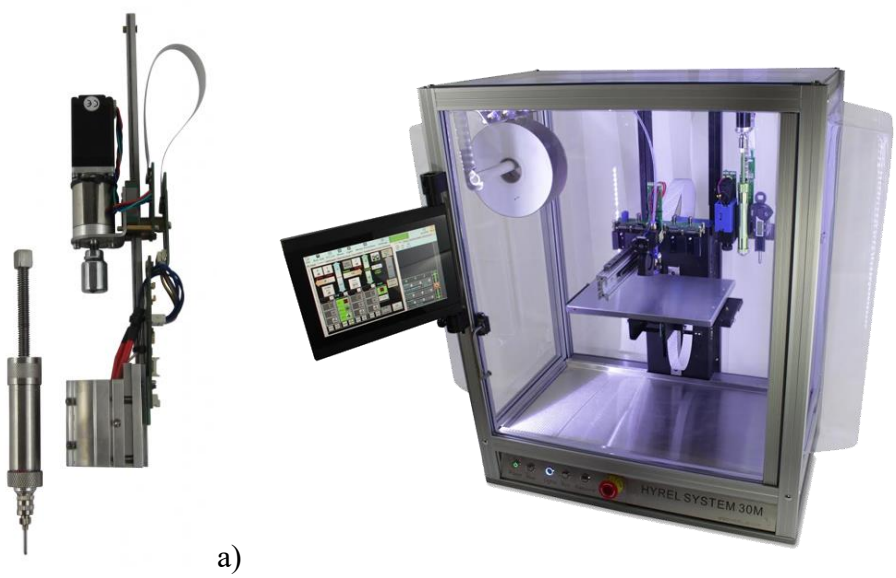

a) b)

Figure 1.15: a) KR2-15 Printhead b) Hyrel System 30M Printer [12]

[12]

The type of specimens printed where tensile testing specimens following ASTM standard d638, standard test method for tensile properties of plastics. This testing standard covers the specimen types for un-reinforced plastic materials using samples shaped as “dog bones”. The dimensions for the tensile specimen type V were the most appropriate for this type of testing and chosen to print the testing specimens.

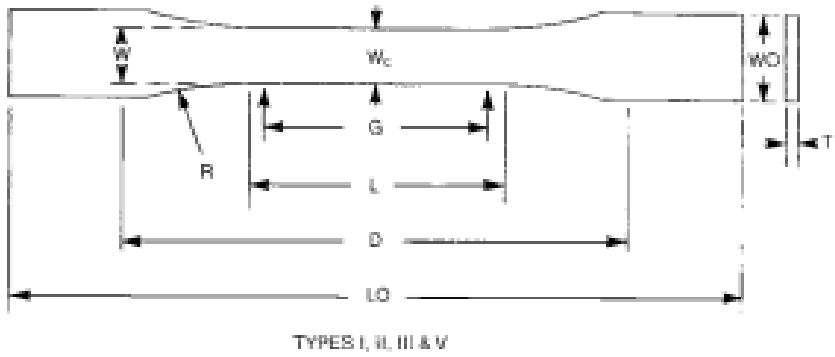

Figure 1.16: Tensile Testing Specimens for ASTM D638[13]

While printing the tensile specimens the infill was selected as rectilinear in the slicer software. The rectilinear infill allowed for an initial vertical infill following the contour shape of the tensile specimen. Once the vertical infill had concluded, it would continue to infill in a horizontal pattern filling the contour of the specimen. This pattern would alternate between vertical and horizontal until the sample had completed printing. Figure 1.17 depicts the printing pattern used for tensile specimens along with the finalized printed green parts.

13

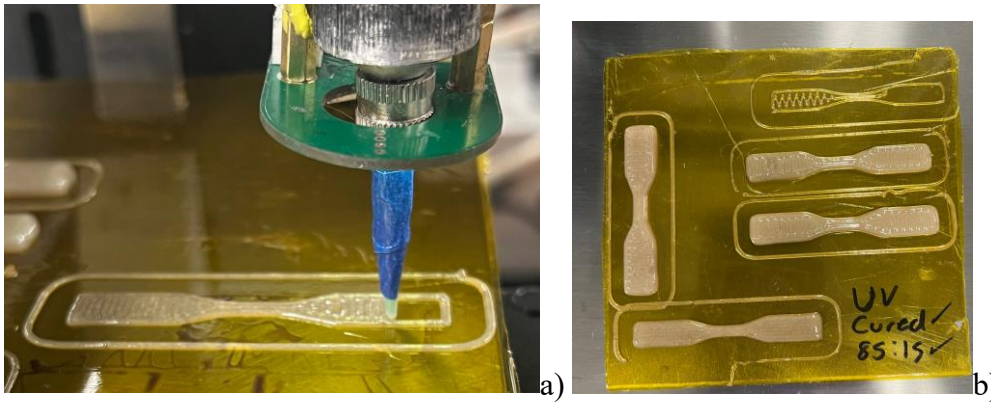

Figure 1.17: a) Printing Pattern b) Finalized Green Part Prints

As previously mentioned, a UV array was mounted directly below the reservoir above the nozzle tip, allowing for early UV curing of the inks. The UV array was mounted by using spacers and screws which directly connected to the reservoir's housing through threaded orifices.

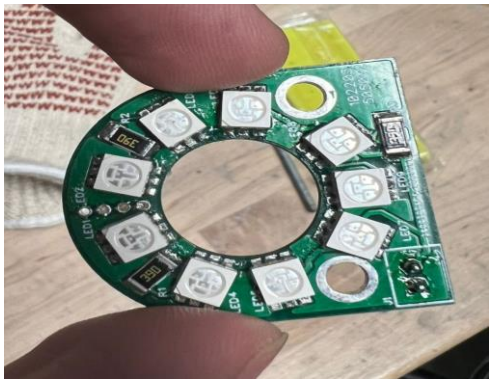
Figure 1.18: Print Head UV Array

Materials where printed on a metal substrate covered in Kapton tape in which they were UV cured for 15 minutes to ensure the proper formation of cross-link networks via UV cure. After completing the UV cure, the materials were applied its regular thermal cure to obtain its desired thermal resistivity properties. Due to the brittleness of the material, after being cured, it was required to heat the samples to a temperature of 100°C for 5 minutes, then separate the samples from the substrate using a blade. If this procedure was not followed it would usually result in the specimens breaking or fracturing, making them unusable for tensile testing.

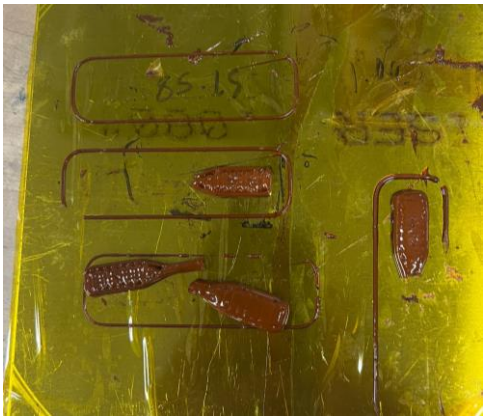

Figure 1.19: Fractured Specimens

Figure 1.20: Successfully Printed Specimens

Tensile Testing at Elevated Temperatures

Tensile testing was done on manufactured 50/50, 70/30, and 85/15 specimens. These specimens were tested under three main temperatures, at room temperature, 100°C and 200°C. All of the testing was performed in an Instron testing load cell of 50 kn. Additionally, an environmental chamber from Instron was used to apply the necessary temperatures to the test. Figure 1.21 shows the testing load cell and environmental chamber used for tensile testing. For specimens tested at 100°C, the samples were allowed to soak in the temperature for 10 minutes. For samples tested at 200°C, the samples were allowed to soak in the temperature for 20 minutes. Upon completion of the soaking times, the specimens were tested.

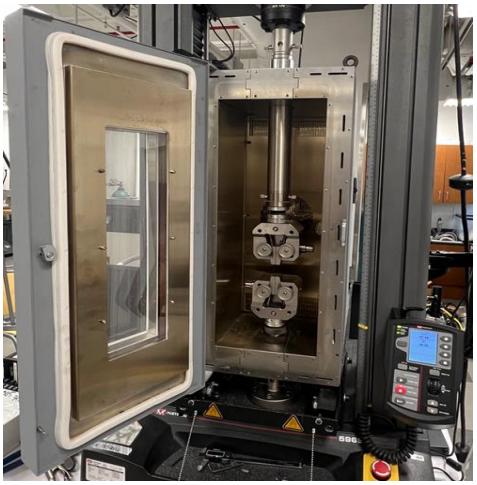

Figure 1.21: Instron Load Cell and Enviromental Chamber

Specimens were tested using the rate of 1 mm/min as specified in ASTM D638. Specimens were marked at the narrow section using a black marker having a length of 9.53mm and at the specified gage length of the specimen using a silver marker by marking dots at the total length of 7.62mm on the middle section. To validate the tensile testing results, it's required for the specimens to fail between the marked gage sections as shown in Figure 1.22. A total of 5 specimens must be tested for each condition and must fail between the marked gage sections for the necessary data under each weight percentage and temperature condition. Necessary dimensions for the testing calculations include the width of the middle section, the thickness of the middle section, the overall length of the specimen, and the fixture separation. Often it was necessary to use sandpaper to achieve an abrasive finish on the specimen; otherwise slipping of the specimen would occur, prolonging the tensile test and giving inconsistent stress vs strain graphs. Figure 1.22 demonstrates a specimen which failed in the appropriate area for the results to be valid.

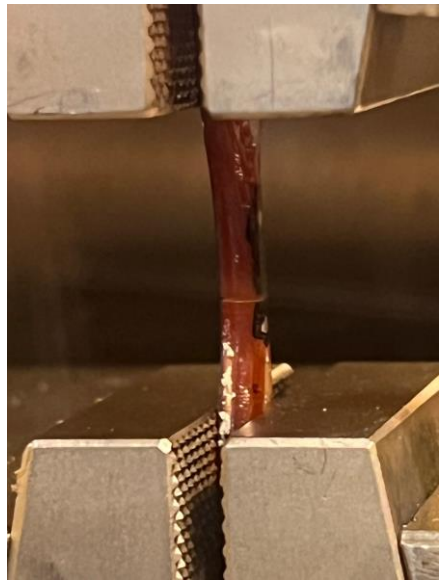

Figure 1.22: Tensile Specimen with Valid Tensile Failure

RESULTS

Testing at Room Temperature

The specimens containing a formulation of 50/50 demonstrated the highest strength at room temperature. The second highest strength was demonstrated by the 70/30 samples. Lastly, the 85/15 samples demonstrated the specimens with the lowest strength. Although, cyanate esters are attributed to having high strengths, the high crosslink structures cause formulations with higher PT-30 content to be more brittle. Although, specimens with lower pt-30 content will not be able to retain their strength at higher temperatures. Table 1.1 displays the average tensile strength results for the specimens tested at room temperature.

Table 1.1: Room Temperature Testing Results

Specimen Formulation (PT-30/Acrylate)	Tensile Strength (MPa)
50/50	57.36
70/30	29.73
85/15	14.16

Testing at 100°C

As previously stated, 50/50 specimens were the strongest at room temperature testing; however, these specimens lose their strength drastically as it is exposed to higher temperatures by losing 53% of its original strength. The specimens with a formulation of 70/30, was able to retain its strength by losing only 4.2% of its original strength. Lastly, specimens with a formulation of 85/15 saw a surprising increase in strength by 50%. These are attributed to the softening of the cured polymer allowing for the increased strain without a fracture occurring. This is further confirmed by specimens obtaining a lower modulus at higher temperature exposures, which further decreases the stiffness of the materials. Results are shown in Table 1.2

Table 1.2: 100°C Testing Results

Specimen Formulation (PT-30/Acrylate)	Tensile Strength (MPa)
50/50	27.12
70/30	28.48
85/15	21.23

Testing at 200°C

Specimens with a 50/50 formulation continue to lose its strength, although at 200°C much more strength is conserved as theses specimens lost 3.58% from the original average strength obtained from the testing at 100°C. The 70/30 specimens were able to retain their strength by only losing 6.74%. Lastly, the 85/15 specimens experienced a higher lose in its strength at it has previously increased during the testing at 100°C. Ultimately the specimens with higher PT-30 content still fail due to its brittle nature. Testing results are recorded in Table 1.3.

Table 1.3: 200°C Testing Results

Specimen Formulation (PT-30/Acrylate)	Tensile Strength (MPa)
50/50	26.15
70/30	26.56
85/15	16.32

CONCLUSION

In conclusion, high performance resins such as phenolic cyanate esters were successfully printed with the addition of fillers. These fillers allowed for the formation of an inter-penetrating network, further adding new functionalities to the high-performance thermosets. By introducing the correct fillers, the thermoset resin was successfully printed while retaining its shape by in-situ UV curing, followed by a thermal cure to obtain the desired thermal properties. Furthermore, specimens with different formulations were thermo-mechanically characterized. The different ink formulations demonstrated a competitive thermal resistance as compared to pure PT-30 with added functionalities. Specimens having a 50/50 formulation demonstrated the best printing accuracy characteristics along with superior tensile properties at room temperature. Specimens at 70/30 combined geometric accuracy, strength, and thermal resistivity, being the best overall ratio. 85/12 specimens demonstrated interesting behavior by seeing an increase in tensile strength and higher thermal stability at elevated temperatures, although much of the geometric accuracy is lost during printing. This work successfully represents the ability for thermosets to be modified for additive manufacturing technologies with similar thermal performance.

FUTURE WORK

Future work recommends the inclusion of strength-enhancing fillers, which counter the brittle properties of the high temperature cyanate ester resins. Recommended strength enhancing fillers include milled carbon fiber, chopped carbon fiber, or continuous carbon fiber. These carbon fiber fillers will additionally contribute to the thermal stability of these suggested

composite materials through DIW. Figure 1.23 demonstrates some test prints using 0.5% of milled carbon fiber added to 85/15 ink.

Figure 1.23: DIW Specimens with Added Milled Carbon Fiber

Chapter 2: Non-Destructive Evaluation and Testing of Carbon Fiber Curved Composites

INTRODUCTION

Non-destructive testing (NDT) is a process of inspecting, testing, or evaluating individual parts or parts of larger assemblies without destroying or rendering them unusable. This allows for the parts to continue being used after the inspection is complete. Typically, these technologies are used to find a variety of characteristics inside inspected materials. Some characteristics include mapping corrosion inside the material, discontinuities, delaminations, finding cracks in the material, or discovering foreign objects trapped inside the material. Currently in industry there are several methods of NDT which allows for a greater quality control in manufactured materials and an ease of inspection without destroying the material. Furthermore, this allows to inspect the integrity of the material to ensure its reliability and safety while in application.[14]

There is a wide range of NDT technologies including radiographic testing (RT), infrared testing (IR), electromagnetic testing (ET), vibration analysis (VA), and ultrasonic testing (UT) to mention a few. During this chapter ultrasonic testing will be discussed in detail.

In UT inspection technologies, an ultra-high frequency noise signal is outputted by the inspection probe, which travels through the inspected material. Once these materials encounter a foreign boundary, for instance air, the signal will bounce back to the probe from which an image is generated from the data collected. These signals are produced using the piezoelectric component which is housed in the scanning probe. As a voltage is applied to the piezoelectric component, it generates a sound wave which travels through the material. This signal bounces back to the probe which generates the image of the scan. The probe is able to find defects or flaws in the composite as the signal is reflected once it meets the discontinuity in the material or defect, part of the reflected energy will travel back to the probe generating a reading which characterizes the defect, while the remaining energy will travel the rest of the inspected material

---

14

and bouncing to the probe once it meets a boundary. Figure 2.1 shows a schematic which further represents the mechanisms in which the UT system detect defects. Some of the typical coupling fluids used for UT include water, oil, and gel.

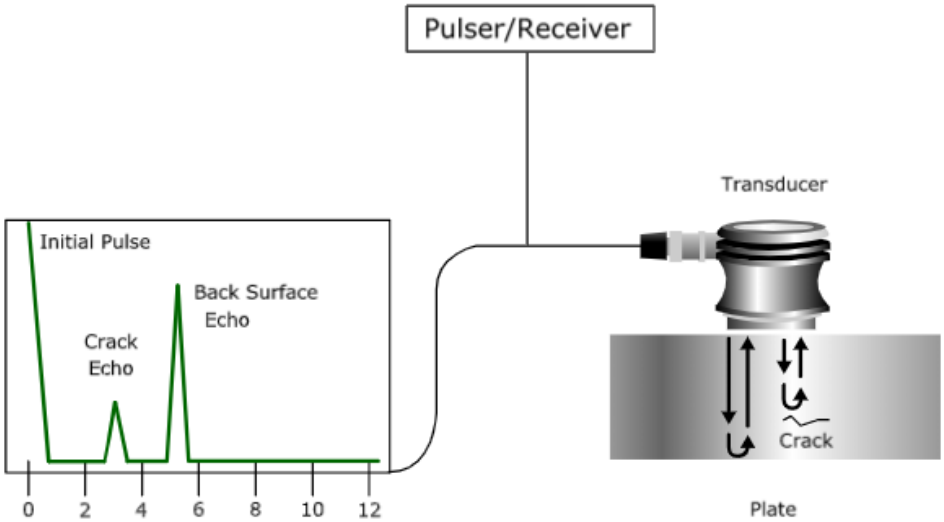

Figure 2.1: NDT Schematic[15]

The goal of this project is to create an artificial intelligence model which is able to identify the depth, location, and defect type of curved composite materials. This is done to further decrease the cost and inspection time from manual inspection, which often requires an export for it to be accomplished. Furthermore, the visualization and characterization of defects will be explored in curved composite materials using C-Scan and B-Scan reading.

EXPERIMENTAL METHODS

Composites Manufacturing

Curved composites were manufactured by manual hand layup and cured at room temperature by vacuum bagging molding. Additionally, a curved mold was printed using FDM technologies to shape the composite to its desired curve. The mold was around 30 inches in length and around 30 inched in width, with a height of a round 5 inches. Two parts of the mold

15

were printed to achieve a superior surface finish which matched the desired curvature. The CAD model represented in Figure 2.2 demonstrate the dimensions and geometry of the printed mold.

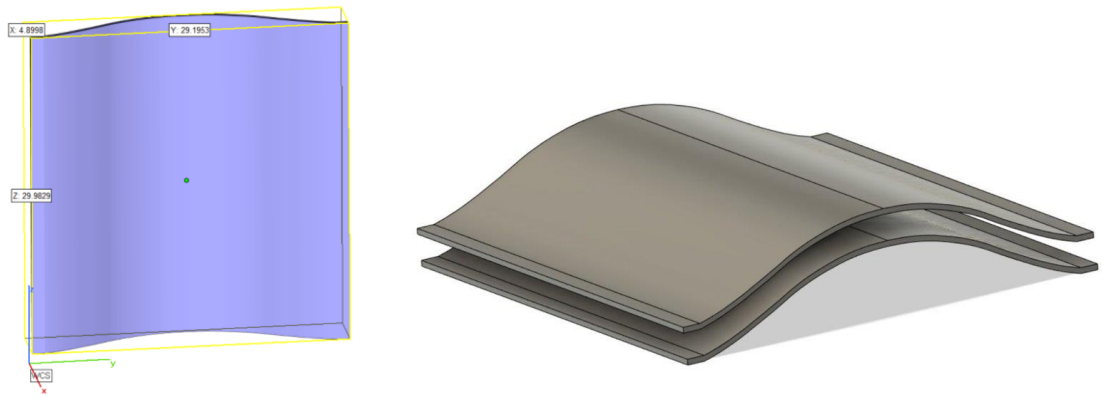

Figure 2.2 Composite Mold CAD Models

Layers utilized for the composite layup included nylon bagging, release film, breather film, and the unidirectional carbon fibers for the composite material. The release film served as a releasing media from the mold while giving a glossy surface finish to the carbon fiber composite which influences the quality of the collected scan data. The breather film was used as an air path for air to consistently flow out of the vacuum bagging enclosure. Lastly, the vacuum bagging along with a, through bag connector, and a vacuum pump, removed the air trapped inside the vacuum bagging allowing for atmospheric pressure to consolidate the composite fibers and remove excess resin. Unidirectional carbon fibers were used for the manufacturing of composites along with an epoxy-based resin along with a room temperature cure catalyzer. Dry fibers hand-layup was chosen as the manufacturing method as the size of the mold and vacuum bagging was much larger compared to the available curing ovens at the research facility. However, due to good craftmanship practices, composite panels with great quality, and surface finishes were manufactured. Figure 2.3 Represents the final vacuum bagging set-up with vacuum being applied.

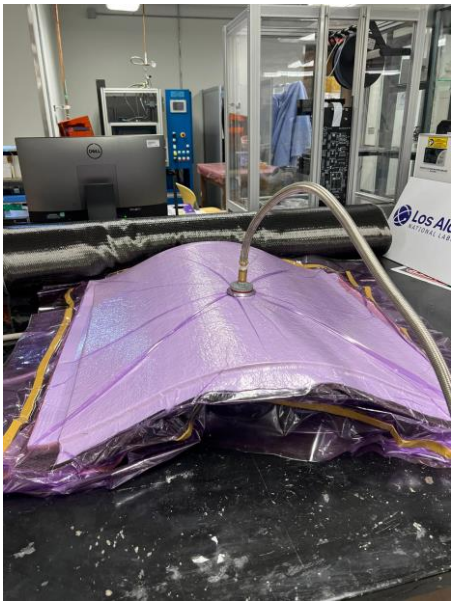

Figure 2.3 Composite Layup with Vacuum Applied

Composites were manufactured at a variety of layers ranging from 10 to 26 carbon fiber layers to investigate the representation of defects in scans based on the thickness and number of layers. Composites having the dimensions of 30” x 30” were initially manufactured with embedded defects such as inclusions and delaminations. Although, later composites were manufactured with the dimensions of 30” x 12” to further improve the manufacturing process and quality of the composite. Inclusion defects were replicated by placing foreign materials such as metal washers between the layers of the composite. Delamination defects were replicated by placing Teflon disks between the layers of the composite. Figure 2.4 demonstrates the embedded defects between the carbon fiber layers. After completing the composite layup, the vacuum was allowed to run for 24 hours until the composite piece was fully consolidated and cured.

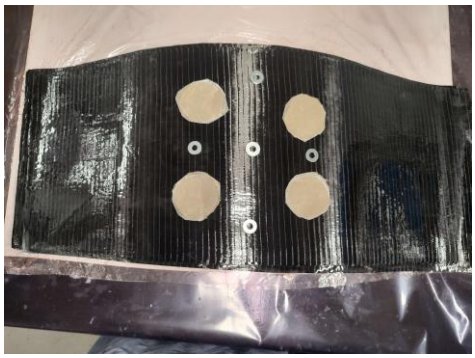

Figure 2.4: Carbon Fiber Composite Embedded Defects

Figure 2.5 demonstrates some of the manufactured composites from which data was gathered to train the artificial intelligence model on.

Figure 2.5: Manufactured Carbon Fiber Composites

Ultrasonic Testing Equipment

The Omniscan SX system from Olympus was used to take all the UT readings. Readings from the Omniscan were taken using a gain between 10 to 16 dB as the best results could be observed at this range. The selected probe to scan the curved composites was the NW-1 phased array probe, which specialized in the detection of delaminations, voids, and disbands. The NW-1 was connected along with a wedge and an encoder wheel. The wedge served as the coupling device between the probe and the encoder wheel. The main purpose of the encoder wheel is to track the distance that the probe has traveled, which contributes to the accurate mapping of the scan data. Figure 2.6 shows the inspection probe and its components.

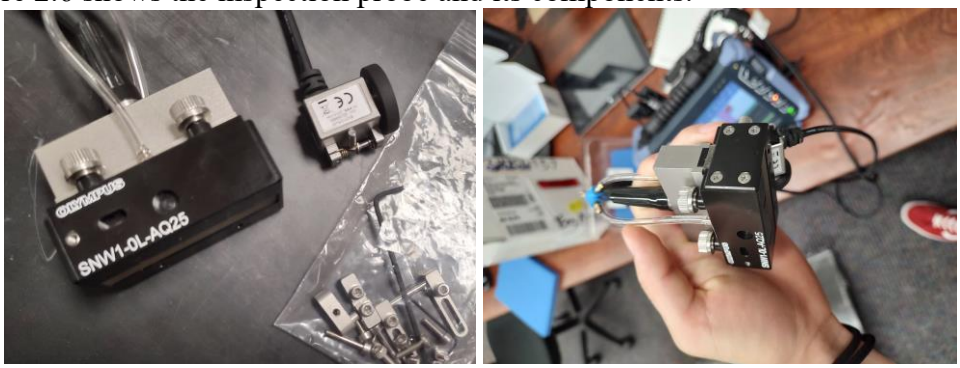

Figure 2.6: NW-1 Probe and its Components

RESULTS

The following images are produced by the collected data from the Omniscan system. Figure 2.7 shows a screen capture of the scans produced by the Omniscan system The top left image displays a C-Scan which is a representation of the top to bottom view of the composite based on the collected raster scans. The inclusion defects are found in the C-Scans represented as yellow, green, and blue colored circles. Bounded in red squares are the detect inclusion defects. Below the C-Scan is the B-Scan which represents a side view of the composite materials cross section. The B-Scan displays an initial top wall being the top surface of the scanned material and a bottom wall being the boundary at which the signal returns to the probe. Although, in this specific section of the B-scans, defects were not detected and hence not displayed in the cross-section of the B-Scan.

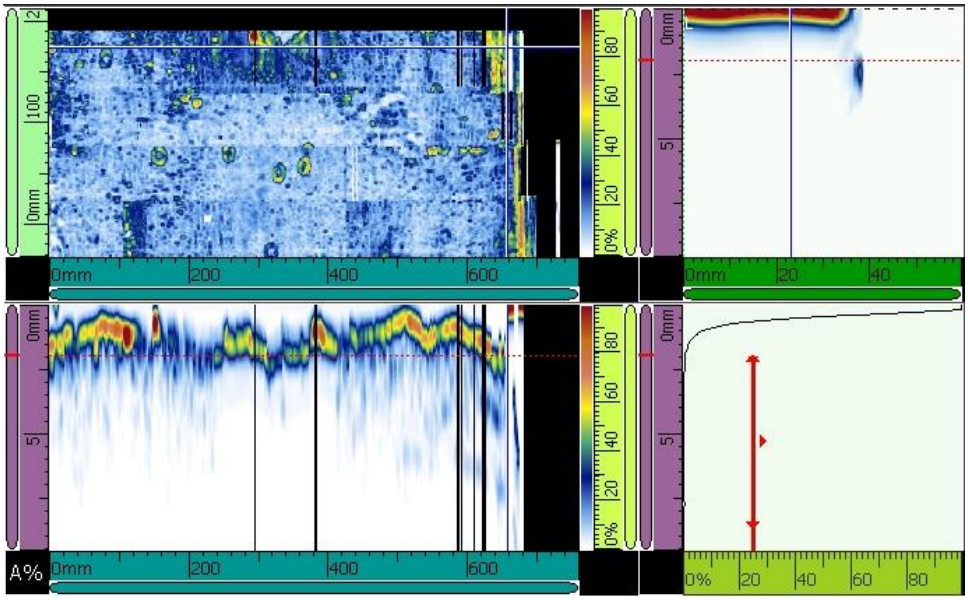

Figure 2.7: Omniscan Scan Readings

Data was exported and reprocessed to generate an image based on the values given by the text file. Figure 2.8 shows the processed B-Scan images which better display the top wall, end wall, and defects found in the cross-section of the object. While exporting the B-Scan data, a total of 100 to 400 images can be generated based on the dimensions of the scanned object.

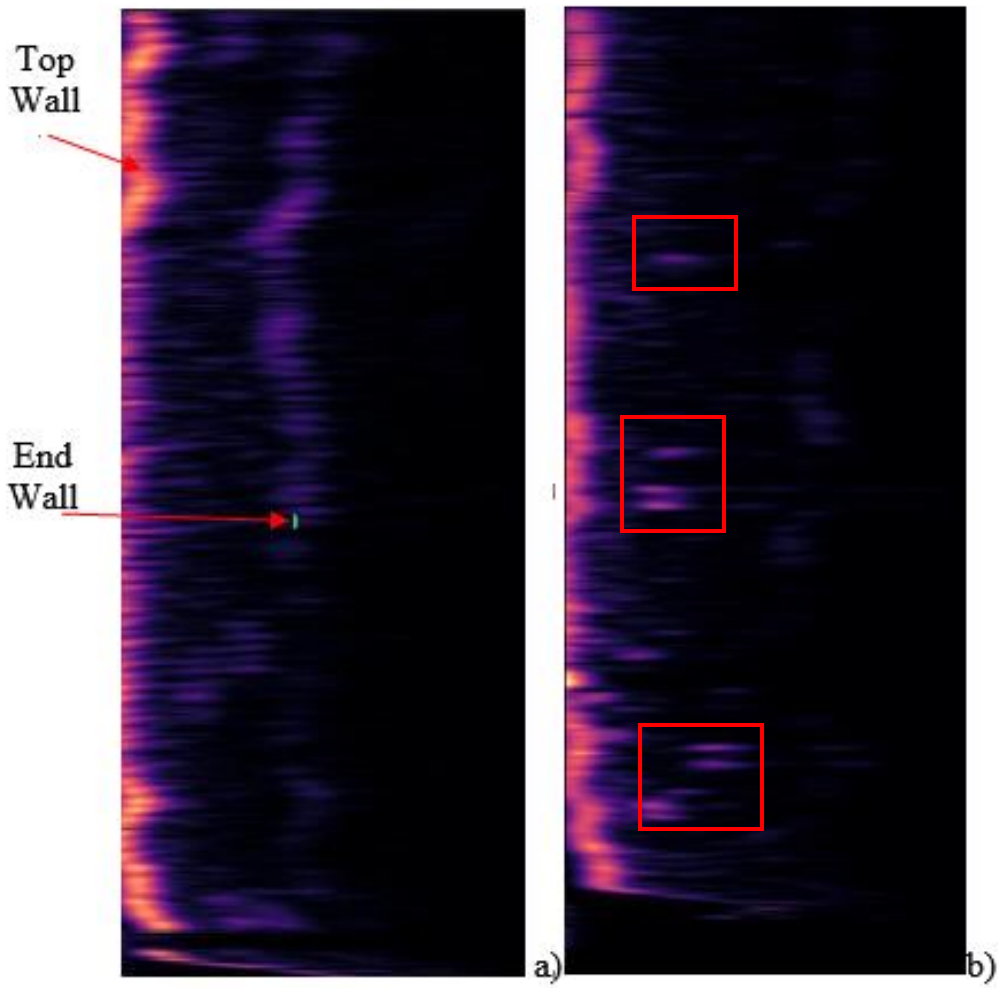

Figure 2.8: a) B-Scan Displaying Walls b) B-Scan Displaying Defects

After generating the images from the exported data, the images were then labeled using a MATLAB application known as Image labeler. The image labeler allows for the creation of different object categories followed by bounding these objects in the image. The labels used for the labeling include wall, inclusion defect, and delamination defect. The exported labels then create a matrix of values indicating the section in which the wall is found or where the defect type is found. Figure 2.9 shows the display in MATLAB, in which a collection of images generated from the B-Scan are manually labeled to train the AI model.

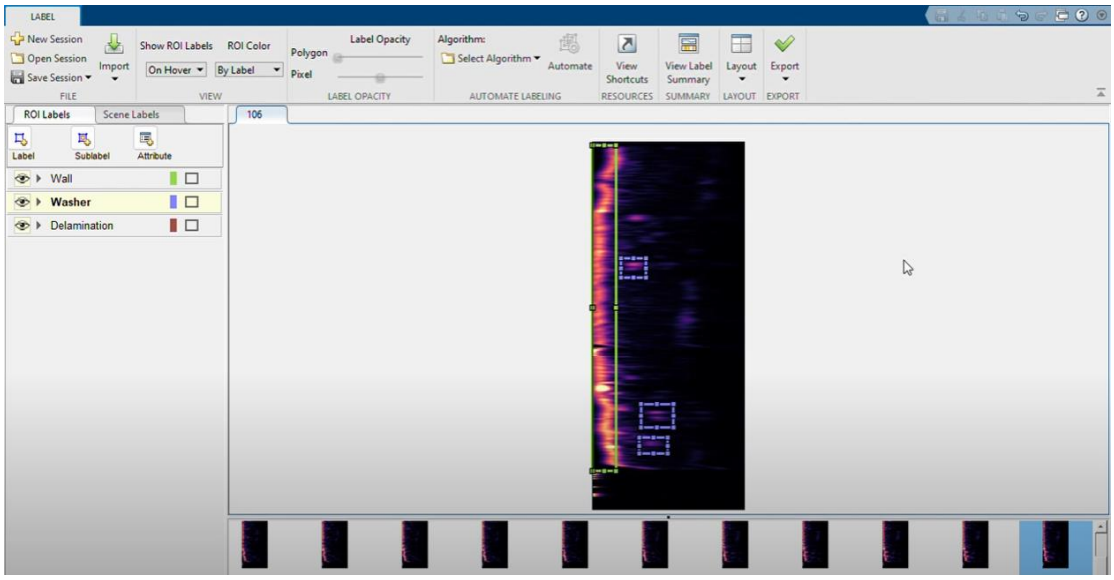

Figure 2.9: Image Labeling Process

Lastly, the model is trained based on the collected data form the image labeling, and tested on its defect detection by using scan images which were not used for the training of the model. The model then bounds the defect or wall found in the scanned images and assigns it a certainty score. The visuals in Figure 2.10 show how the model detects the defects shown in the scans and the various certainty scores assigned for each detection.

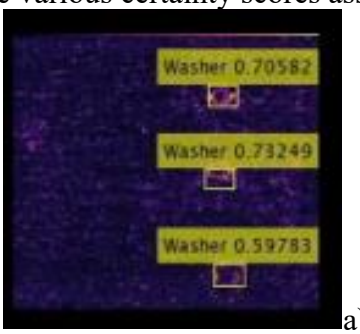

a)

b)

Figure 2.10: a) Defect detection in the C-Scan b) Defect and Wall detection in the B-Scan

CONCLUSION

In conclusion, curved composites with intentional defects were successfully manufactured through methods of manual hand-layup and vacuum bagging curing. Both the delamination defects and inclusion defects were properly detected using UT technologies and visible for the inspectors to detect and label data to train the artificial intelligence algorithm. The

AI model successfully detected defects from the validation data, being able to find inclusion and delamination defects for the C-Scan while detecting walls, inclusions, and delaminations for the B-Scan. This work has successfully achieved the building of an artificial intelligence model being able to detect defects in a composite.

FUTURE WORK

Although the artificial intelligence model was able to detect inclusion and delamination defects, some areas to expand include the replication of porosity defects and wrinkles occurring during the manufacturing process. Porosity and wrinkles are proposed as the next steps for the project as there are some of the most common types of defects which occur in industry. Furthermore, the team continues to work on the visualization of this model for curved composites using tools such as unity. This will allow for shorter inspection times and a better understanding to the location and depth of defects in composite materials.

References

[1] Washington State University. (n.d.). *Fundamentals of Direct-Ink-Writing*. WSU Labs. Retrieved December 9, 2022, from https://labs.wsu.edu/mpml/projects/

[2] Zhang, B., Chung, S. H., Barker, S., Craig, D., Narayan, R. J., & Huang, J. (2021). Direct ink writing of polycaprolactone / polyethylene oxide based 3D constructs. *Progress in Natural Science: Materials International*, *31*(2), 180–191. https://doi.org/10.1016/j.pnsc.2020.10.001

[3] Saadi, M. A., Maguire, A., Pottackal, N. T., Thakur, M. S., Ikram, M. M., Hart, A. J., Ajayan, P. M., & Rahman, M. M. (2022). Direct ink writing: A 3D printing technology for diverse materials. *Advanced Materials*, *34*(28), 2108855. https://doi.org/10.1002/adma.202108855

[4] Olivera, S., Muradlihara, H. B., & Venkatesh, K. (2016, January). *Evaluation of surface integrity and strength characteristics of …* Retrieved December 9, 2022, from https://www.researchgate.net/publication/292985550_EVALUATION_OF_SURFACE_INTEGRITY_AND_STRENGTH_CHARACTERISTICS_OF_ELECTROPLATED_ABS_PLASTICS_DEVELOPED_USING_FDM_PROCESS

[5] Khan, S. A., & Lazoglu, I. (2019). Development of additively manufacturable and electrically conductive graphite–polymer composites. *Progress in Additive Manufacturing*, *5*(2), 153–162. https://doi.org/10.1007/s40964-019-00102-9

[6] Karuppiah, A. (2016, December). *(PDF) predicting the influence of weave architecture on … - researchgate*. PREDICTING THE INFLUENCE OF WEAVE

ARCHITECTURE ON THE STRESS RELAXATION BEHAVIOR OF WOVEN COMPOSITE USING FINITE ELEMENT BASED MICROMECHANICS. Retrieved December 9, 2022, from https://www.researchgate.net/publication/329156276_PREDICTING_THE_INFLUENCE_OF_WEAVE_ARCHITECTURE_ON_THE_STRESS_RELAXATION_BEHAVIOR_OF_WOVEN_COMPOSITE_USING_FINITE_ELEMENT_BASED_MICROMECHANICS

[7] Plastics, A. (2022, July 13). *Thermoset vs thermoplastic*. Thermoset Vs Thermoplastic. Retrieved December 9, 2022, from https://adrecoplastics.co.uk/thermoset-vs-thermoplastic/

[8] Technologies, A. E. M. C. (2017, April 28). *Understanding the glass transition temperature of polymers - advanced EMC technologies: High performance polymer seals & bearings*. Advanced EMC Technologies | High Performance Polymer Seals & Bearings. Retrieved December 9, 2022, from https://advanced-emc.com/glass-transition-temperature-of-polymers/

[9] Ramirez, M. L., Walters, R., Lyon, R. E., & Savitski, E. P. (2002). Thermal decomposition of cyanate ester resins. *Polymer Degradation and Stability*, *78*(1), 73–82. https://doi.org/10.1016/s0141-3910(02)00121-0

[10] Hedstrom, J. (2017, November 23). *3D printing with Carbon's cyanate ester: The complete Q&A*. Sculpteo. Retrieved December 9, 2022, from https://www.sculpteo.com/blog/2016/06/01/3d-printing-with-carbons-cyanate-ester-the-complete-qa/

[11] Zhou, Z.-X., Li, Y., Zhong, J., Luo, Z., Gong, C.-R., Zheng, Y.-Q., Peng, S., Yu, L.-M., Wu, L., & Xu, Y. (2020). High-performance cyanate ester resins with interpenetration

networks for 3D printing. ACS Applied Materials & Interfaces, 12(34), 38682–38689. https://doi.org/10.1021/acsami.0c10909

[12] Hyrel 3D. (n.d.). System 30M 3D printer. Hyrel3D. Retrieved December 9, 2022, from https://www.hyrel3d.com/portfolio/system-30m/

[13] ASTM International. (n.d.). *Standard test method for tensile properties of plastics*. ASTM International - Standards Worldwide. Retrieved December 9, 2022, from https://www.astm.org/d0638-14.html

[14] American Society for Nondestructive Testing. (n.d.). *INTRODUCTION TO NONDESTRUCTIVE TESTING*. Introduction to nondestructive testing. Retrieved December 9, 2022, from https://www.asnt.org/MajorSiteSections/About/Introduction_to_Nondestructive_Testing.aspx#:~:text=Nondestructive%20testing%20(NDT)%20is%20the,part%20can%20still%20be%20used.

[15] Iowa State University Center for Nondestructive Evaluation. (n.d.). *Basic principles of ultrasonic testing*. Nondestructive Evaluation Techniques: Ultrasound. Retrieved December 9, 2022, from https://www.nde-ed.org/NDETechniques/Ultrasonics/Introduction/description.xhtml

Vita

Sergio Dante Favela completed his Bachelor of Science in Mechanical Engineering at the University of Texas at El Paso (UTEP) in May of 2021. Currently, Mr. Favela is pursuing a Masters of Science in Mechanical Engineering along with a graduate certificate in 3D engineering and additive manufacturing at UTEP.

Mr. Favela had the opportunity to intern with several companies during his undergraduate and graduate years. He initially interned with Freeport McMomoran in 2019 at their Norwich, Connecticut location. After obtaining his degree from UTEP he completed an internship with Sandia National Laboratories in 2021. Prior to graduating Mr. Favela had the opportunity to intern with Kansas City National Security Campus managed by Honeywell FM&T in 2022.

Mr. Favela had the opportunity to participate in sponsored research from Honeywell FM&T and Lockheed Martin Aeronautics. During his research with Honeywell FM&T he investigated the strength of carbon fiber composites at elevated temperatures using high performance thermosets as the matrix system. For the research with Lockheed Martin Aeronautics, Sergio worked with Non-destructive technologies such as ultrasound scanning to detect defects inside of curved carbon fiber composites.

At this time Mr. Favela has two publications based on previous research involving composites and direct ink write technologies and hopes to publish his thesis topics.

Contact Information (Email): sdfavela@miners.utep.edu